




## Article

# The Formation of Nanoscale Closed Graphene Surfaces during Fullerite C<sub>60</sub> Hot Isostatic Pressing

Danil V. Sivkov<sup>1,2,\*</sup>, Olga V. Petrova<sup>2,\*</sup> , Sergey V. Nekipelov<sup>2</sup>, Alexander S. Vinogradov<sup>1</sup> , Roman N. Skandakov<sup>2</sup>, Ksenia A. Bakina<sup>2</sup>, Sergey I. Isaenko<sup>3</sup>, Anatoly M. Ob'edkov<sup>4</sup>, Boris S. Kaverin<sup>4</sup> and Viktor N. Sivkov<sup>2</sup> 

<sup>1</sup> Faculty of Physics, Federal State Budgetary Educational Institution of Higher Education "Saint-Petersburg State University", 199034 St. Petersburg, Russia; asvinograd@yahoo.de

<sup>2</sup> Institute of Physics and Mathematics, Komi Science Centre of the Ural Branch of the Russian Academy of Sciences, 167982 Syktyvkar, Russia; nekipelovsv@mail.ru (S.V.N.); scanick@yandex.ru (R.N.S.); tylxen@gmail.com (K.A.B.); sivkovvn@mail.ru (V.N.S.)

<sup>3</sup> Institute of Geology, Komi Science Centre of the Ural Branch of the Russian Academy of Sciences, 167982 Syktyvkar, Russia; isaenko@geo.komisc.ru

<sup>4</sup> Hybrid Nanomaterials Laboratory, G.A. Razuvaev Institute of Organometallic Chemistry of the Russian Academy of Sciences, 603950 Nizhny Novgorod, Russia; amo@iomc.ras.ru (A.M.O.); kaverin@iomc.ras.ru (B.S.K.)

\* Correspondence: d.sivkov@spbu.ru (D.V.S.); teiou@mail.ru (O.V.P.); Tel.: +7-812-428-4352 (D.V.S.); +7-821-239-1461 (O.V.P.)



**Citation:** Sivkov, D.V.; Petrova, O.V.; Nekipelov, S.V.; Vinogradov, A.S.; Skandakov, R.N.; Bakina, K.A.; Isaenko, S.I.; Ob'edkov, A.M.; Kaverin, B.S.; Sivkov, V.N. The Formation of Nanoscale Closed Graphene Surfaces during Fullerite C<sub>60</sub> Hot Isostatic Pressing. *Appl. Sci.* **2021**, *11*, 11646. <https://doi.org/10.3390/app112411646>

Academic Editors: Petr Korusenko, Sergey Nesov and Yuri K. Gun'ko

Received: 20 October 2021

Accepted: 30 November 2021

Published: 8 December 2021

**Publisher's Note:** MDPI stays neutral with regard to jurisdictional claims in published maps and institutional affiliations.



**Copyright:** © 2021 by the authors. Licensee MDPI, Basel, Switzerland. This article is an open access article distributed under the terms and conditions of the Creative Commons Attribution (CC BY) license (<https://creativecommons.org/licenses/by/4.0/>).

**Abstract:** The fullerite C<sub>60</sub> modified by hot isostatic pressing (HIP) at 0.1 GPa in argon near and beyond its thermal stability region (920–1270 K temperature interval) was studied by X-ray diffraction, Raman spectroscopy, ultra soft X-ray photoelectron and near edge X-ray absorption fine structure spectroscopy. It was found that the C<sub>60</sub> molecules merge into closed nanocapsules with a graphene surface during the thermal treatment. The conducted studies showed that using HIP treatment of the fullerite C<sub>60</sub>, it is possible to obtain a chemically resistant material with a high hardness and elasticity, as well as a density lower than that of the graphite. This new material, consisting of closed graphene nanocapsules 2–5 nm in size, formed by sp<sup>2</sup> covalent bonds between carbon atoms is promising for various applications, and as a basis for the synthesis of new composite materials.

**Keywords:** XPS; NEXAFS; XRD; Raman spectroscopy; fullerite C<sub>60</sub>; HIP treatment

## 1. Introduction

In this work, for the first time, comprehensive studies of the fullerite C<sub>60</sub> modified by hot isostatic pressing (HIP) were carried out using a complementary set of methods that are informative at the nano and micro levels of the structure of matter. Studies of the behavior of the molecular fullerene C<sub>60</sub> and its condensed phase, fullerite, at high pressures and temperatures began in the mid-1990s, when simple methods for producing C<sub>60</sub> were proposed and it became available in gram quantities [1–3]. Various polymer phases of C<sub>60</sub> and their changes at temperatures above the limit of thermal stability of C<sub>60</sub> were studied [4–8]. The investigations of the fullerene C<sub>60</sub> transformations at high static and dynamic pressures at temperatures above the thermal stability limit of C<sub>60</sub> molecular clusters [9–20] showed great opportunities for the creation of new carbon materials with a wide variety of physicochemical properties. As a result, sufficiently detailed phase diagrams of the fullerene C<sub>60</sub> were obtained, especially at the pressure above 1 GPa [21–23].

At the same time, studies on the intercalation of various gases into the fullerite lattice in gasostats (devices allowing to create high gas pressures up to 300 MPa) at high temperatures (more than 1770 K) were conducted. It was shown, for example, that at temperatures of 400–500 K and the limiting pressures Ar, Xe and Kr fill fullerite octahedral voids, while its face-centered cubic (fcc) structure is preserved [24,25]. Studies of the fullerite

behavior at pressures of 0.1–1.5 GPa and temperatures above the collapse temperature of the  $C_{60}$  molecule [7,16] showed that the resulting disordered nanocarbon phase has unique properties such as high hardness and elasticity at a density lower than that of graphite. Therefore, finding and describing the structural and electron characteristics of fullerite under different external conditions is an important task. In the available works, as a rule, data obtained by separate methods for certain values of pressures and temperatures are given. At the same time, there are no data on XPS and NEXAFS studies of HIP-treated fullerene  $C_{60}$ . This does not allow the objective characterization of the process of the fullerite modification and reliably determines the atomic chemical composition and structure of the final product. It is obvious that further serious progress in the study of solid-phase transformations of  $C_{60}$  is impossible without the use of the modern methods of studying the atomic–electronic properties of such polyatomic systems. The complexity of the nanoscale atomic–electron structure of such materials requires the use of the combination of the complementary research methods. These methods should be highly informative at the nanoscale, non-destructive and highly sensitive to the sample atomic structure and its changes due to physical and chemical influences. The near edge X-ray absorption fine structure (NEXAFS) spectroscopy [26] and X-ray photoelectron spectroscopy (XPS) [27,28] are effective experimental methods that allow us to directly obtain detailed information about the nanoscale atomic–electron structure of the polyatomic system under study. Their combination with traditional Raman spectroscopy and X-ray diffractometry (XRD) provides new reliable knowledge about the atomic and electronic structure of nanostructured carbon materials [29,30]. In this work, the successive modification of fullerite  $C_{60}$ , as a result of HIP at a pressure of 0.1 GPa in an argon atmosphere in the temperature range of 920–1270 K, was characterized by XRD, XPS, NEXAFS and Raman spectroscopy. The study showed that changes in X-ray diffraction patterns, C 1s NEXAFS and Raman spectra appear simultaneously due to structural changes in the fullerite  $C_{60}$  with increasing temperature during HIP treatment.

## 2. Materials and Methods

### 2.1. Materials

Materials list: a 99.98% pure fullerite  $C_{60}$  powder with a crystallite size of 0.05–0.5 nm (produced by Fullerene-Center, Nizhny Novgorod, Russia); gaseous argon (produced by LLC SPE “Salyut-gas”, Nizhny Novgorod, Russia, TU 2114-011-106-818-63-2005) with its volume fraction is not less than 99.994%; multi-walled carbon nanotubes (MWCNTs) with average outer diameter of 80 nm, average length of 300  $\mu$ m, carbon purity of 98 wt.%, Fe-based catalyst residue of (5.5–7.5) wt.% (synthesized in the Hybride Nanomaterials Laboratory of G.A. Razuvaev Institute of Organometallic Chemistry of the Russian Academy of Sciences (RAS)); highly ordered pyrolytic graphite (HOPG) (produced by SPI supplies, West Chester, PA, USA), ZYA grade.

### 2.2. Experimental Details

#### 2.2.1. HIP Treatment

The fullerite  $C_{60}$  sample preparing process consisted of grinding in a mortar with hexane for 20 min and subsequent pressing into tablets with the 20 mm diameter and 3 mm thickness. Then, the samples were subjected to HIP treatment in the gasostat with a multi-level working table for sample placement and thermocouples for temperature control. The synthesis was performed at a constant 0.1 GPa pressure in an argon medium at temperatures of 920, 1120, 1170 and 1270 K and a 3 h exposure time.

#### 2.2.2. Characterization

The pristine fullerite  $C_{60}$  and its samples after HIP treatment were characterized using a number of chemical and physical analysis methods. XRD were conducted using equipment from the Center of “physics and technology of micro- and nanostructures” at the Institute for Physics of Microstructures of RAS and Raman Spectroscopy—using

equipment from the Center of Collective Use at the Institute of Geology of Komi Science Center of the Ural Branch of RAS.

XRD analysis of the pristine C<sub>60</sub> powder and HIP-treated materials was performed with CuK<sub>α</sub>-radiation using a Bruker D8 Discover X-ray diffractometer (Bruker Corp., Billerica, MA, USA) in the  $\theta$ -2 $\theta$  symmetrical geometry with a Gobel mirror, an equatorial Soller slit with the angular divergence of 2.5°, and a slit of 1.5 mm on the primary beam. The obtained diffraction patterns were processed using DIFFRAC.EVA V.3.0 software (Bruker Corp., Billerica, MA, USA) with the PDF-2 (2012) powder diffraction database.

Raman studies were conducted at room temperature using an Ar laser with the 1 mW power and 488 nm wavelength. Spectra were recorded using a monochromator with the 600 lines/mm diffraction grating in the 100–4000 cm<sup>-1</sup> range. The spatial and spectral resolution was 1  $\mu$ m and 1 cm<sup>-1</sup>, respectively. Each spectrum was the result of three accumulations with a 10 s exposure. The spectra fitting was performed by LabSpec V.5.36 software (Horiba, Ltd., Kyoto, Japan).

All NEXAFS spectroscopy data were obtained at the Berliner Elektronenspeicherring für Synchrotronstrahlung (BESSY II), Helmholtz-Zentrum, Berlin, Germany, using synchrotron radiation (SR) of the Russian–German beamline (RGL) [31,32]. C 1s NEXAFS spectra were measured using total electron yield (TEY) mode with correct consideration of non-monochromatic background and instrumental distortions. For energy calibration of these spectra, the energy positions of the first- and second-order light-excited Au 4f<sub>7/2</sub> photoelectron (PE) lines were used. The spectral variation of the photon flux was measured by recording a TEY signal from a clean Au plate. The photon energy resolution in the vicinity of the C 1s (~280 eV) absorption edge was set to 50 meV.

XPS studies were carried out using an ESCALab 250Xi X-ray photoelectron spectrometer (Thermo Fisher Scientific, Waltham, MA, USA) with AlK<sub>α</sub> radiation (1486.6 eV) of X-ray tube to excite PE spectra at room temperature equipped with the electron-ion sample charge compensation system (the resource center in the Science Park at St. Petersburg State University, “physical methods for surface research”). The C 1s and O 1s core level and survey PE spectra were obtained with a total energy resolution of about 0.3 eV at the pass energy of 50 eV and 100 eV, respectively. The experimental particularities and the used equipment characteristics are described in more detail elsewhere [29,33]. Samples for XPS and NEXAFS spectroscopy were prepared by pressing fullerene powder into the copper plate surface.

All Raman, NEXAFS, and XPS measurements were performed for a series of samples at different points for each one, and their results had good reproducibility.

### 3. Results and Discussion

#### 3.1. Pristine Fullerite C<sub>60</sub> Study

The results of preliminary tests of the initial powder of pristine fullerene C<sub>60</sub> by XRD, Raman, XPS and NEXAFS techniques are shown on Figure 1a–c and Figure 1d, respectively. The XRD patterns (Figure 1a) are in good agreement with those of the studies [34–36] and Raman spectrum (Figure 1b) show only the peaks characteristic of pure C<sub>60</sub> [21,36–38].

Figure 1c shows the overview XPS spectra in the 0–1200 eV binding energy (BE) range for the C<sub>60</sub> powder and highly oriented pyrolytic graphite (HOPG) exposed to air for a long time. This spectrum of the C<sub>60</sub> powder contains an intense C 1s peak at 284.7 eV (full width at half maximum, FWHM is 1.3 eV) and a broader O 1s line at 532.2 eV (FWHM is 2.6 eV). In turn, the HOPG spectrum is also characterized by an intense C 1s peak at 284.6 eV (FWHM is 1.1 eV) and a broader O 1s line at 532.0 eV (FWHM is 2.4 eV). XPS measurements allow to derive an estimate of the oxygen relative atomic concentration on the C<sub>60</sub> powder surface, equal to 4%, and on the HOPG surface, equal to 8%. The availability of the O 1s peak in the overview XPS spectra of C<sub>60</sub> and HOPG indicates the presence of oxygen-containing compounds on the surface of the materials under study. Possible reasons for this could be carbon oxides, as well as water and oxygen molecules physically adsorbed from the air. The inset in Figure 1c shows C 1s and O 1s core-level PE

spectra of C<sub>60</sub> and HOPG. In both of C 1s spectra there is only one asymmetric peak and no signals associated with carbon oxides. The main line of the C 1s core level PE spectrum of HOPG is accompanied by a noticeable tail on the high-energy side, which is caused by  $\pi$ -type shake-up satellite [39–41].

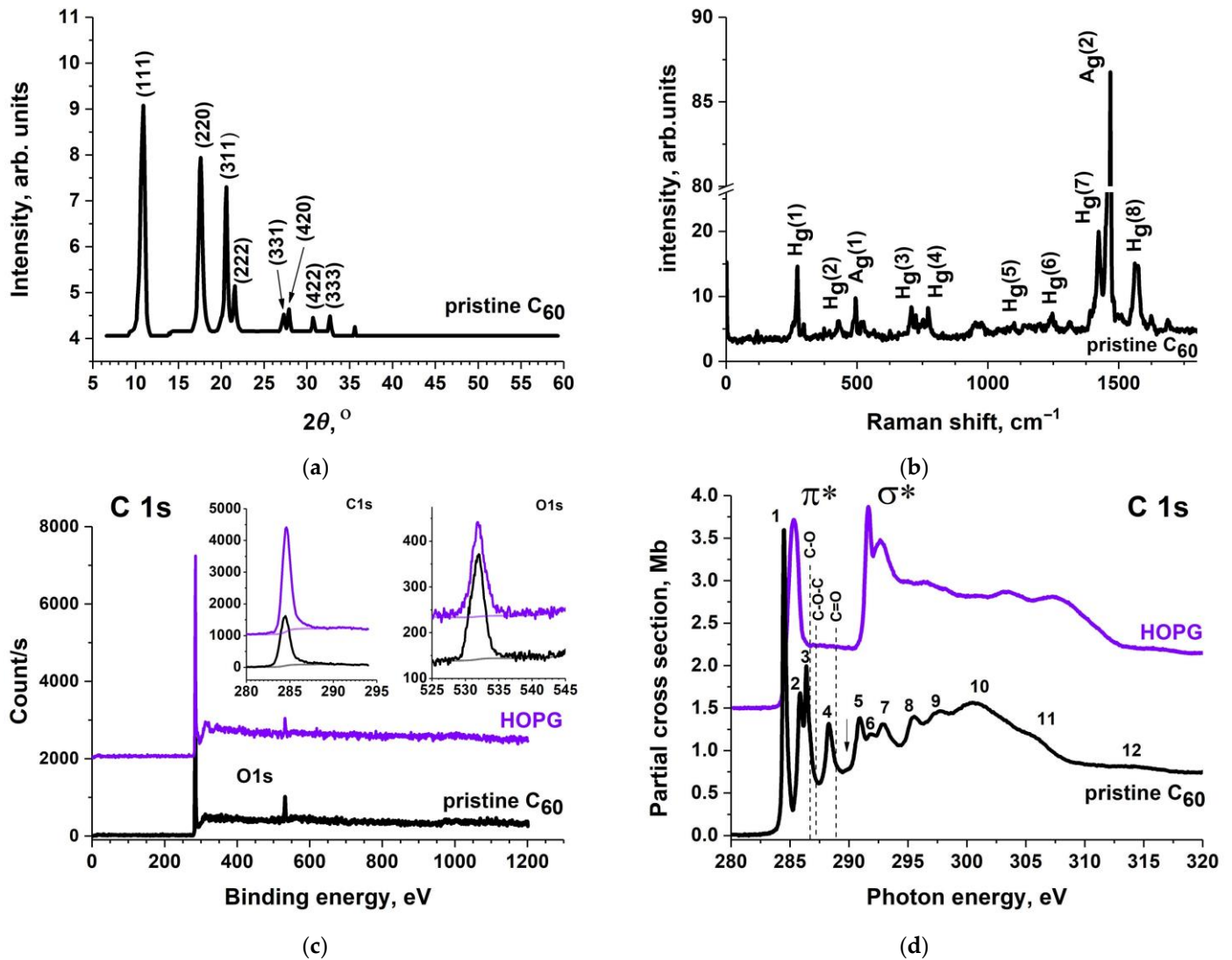


**Figure 1.** Characterization of the pristine C<sub>60</sub> powder and HOPG: (a) C<sub>60</sub> XRD pattern; (b) C<sub>60</sub> Raman spectra; (c) survey XPS spectra of the C<sub>60</sub> and HOPG, the inset shows their C 1s and O 1s XPS spectra; (d) C 1s NEXAFS spectra of the C<sub>60</sub> and HOPG (shifted at the vertical scale by 1.5 Mb). The arrow in (d) indicates the position of the fullerite C<sub>60</sub> C 1s absorption edge (289.60 eV) [42]. The positions of the absorption bands in the atomic groups C=O (288.9 eV), C–O–C (287.2 eV) and C–O (286.7 eV) [43] are marked with dashed lines.

The obtained C 1s NEXAFS spectra of HOPG and C<sub>60</sub> in terms of the number of absorption bands and their energy positions are in good agreement with the results of the previous works [42,44–51], respectively. The presence of carbon oxides on the fullerite C<sub>60</sub> and HOPG surface can be detected using the C 1s NEXAFS spectra shown in Figure 1d. The energy positions of absorption bands in the C 1s NEXAFS spectrum of the fullerite C<sub>60</sub> are given in Table 1.

**Table 1.** Energy positions of absorption bands in C 1s NEXAFS spectrum of C<sub>60</sub>.

Peak Number	1	2	3	4	5	6	7	8	9	10	11
Photon energy, eV	284.50	285.84	286.43	288.30	290.91	291.85	292.93	295.50	297.50	300.73	~305.50



At room temperatures fullerene  $C_{60}$  condenses into a molecular crystal (fullerite  $C_{60}$ ) in which the molecules are bound by weak Van der Waals forces and are in quasi-free rotational motion. This crystal has an fcc lattice with a 1.417 nm lattice constant and 1.002 nm intermolecular distance [36]. The C 1s NEXAFS studies of  $C_{60}$  in condensed and gaseous phases [50], as well as  $C_{60}$  molecules isolated in the Xe matrix [51] showed that intermolecular interaction in fullerite  $C_{60}$  does not play a significant role in the formation of its electronic structure and the electron correlation effects are intramolecular. It was also found [51] that the BE of C 1s electron in crystalline fullerite is 0.4 eV less than in the gas-phase  $C_{60}$  molecule. It should also be emphasized that the shape and energy positions of absorption bands in the C 1s NEXAFS spectra of crystalline and molecular  $C_{60}$  coincide. This is evidence for a negligible effect of neighboring molecules on the C 1s NEXAFS spectrum due to the weakness of intermolecular interactions. Therefore, the calculation data for the  $C_{60}$  cluster can be used to interpret the C 1s NEXAFS spectrum of fullerite [34]. The icosahedral-symmetric  $C_{60}$  theoretical study [34] shows the expediency of extending the Hückel molecular orbital method, previously used for planar conjugate systems (where each carbon atom forms three two-electron localized  $\sigma$ -bonds with neighboring atoms, and the fourth electron is located on the  $\pi$ -orbital orthogonal to the three  $\sigma$ -orbitals), to large spheroidal molecules. The  $C_{60}$  molecular structure has the non-planar (pyramidal) atom arrangement. This affects the  $\pi$ -orbital nature and leads to the presence of frame stresses and decreases the fullerene thermodynamic stability compared to graphite [52]. It should be noted that the  $\pi$ - and  $\sigma$ -orbital approximation for the  $C_{60}$  molecule is not strict. However, for large surfaces, the  $\pi$ -like orbitals are oriented close to the normal to the surface, and  $\sigma$ -like—tangential to the surface.

In the literature, there are extensive data on the nature of the C 1s NEXAFS spectrum of the  $C_{60}$  fullerene molecule, theoretically calculated in various approximations [34,52–54]. On their basis peaks 1–4 (Figure 1d) can be identified as a result of C 1s electron transitions to the unoccupied molecular orbitals (MO) of  $t_{1u}$ ,  $t_{1g}$ ,  $h_g$  and  $t_{2u}$  symmetry, respectively. The structures 5–11 above the C 1s ionization threshold are not unambiguously identified at present. However, the band structure calculations for the fullerite  $C_{60}$  with an fcc lattice within the density functional theory [55] showed that the  $\pi$ -zones are located in the range of BE from  $-6$  eV to  $+7$  eV, and the bonding and antibonding  $\sigma$ -states are located lower and higher on the energy scale, respectively. Thus, sharp peaks 5–8 can be attributed to C 1s electron transitions to the  $\pi^*$  MOs, and broad bands 9–11 to those to  $\sigma^*$  MOs.

The vertical dashed lines in Figure 1d indicate the positions of the peaks corresponding to C 1s  $\rightarrow \pi^*$  transitions in the atomic groups C=O (288.9 eV), C–O–C (287.2 eV) and C–O (286.7 eV) [43]. The Figure 1d clearly shows the absence of such features in the C 1s NEXAFS spectra of the  $C_{60}$  and HOPG. This indicates that the above O 1s XPS peaks are related to oxygen and water molecules physically adsorbed on the surfaces of  $C_{60}$  and HOPG without the formation of an oxygen-carbon chemical bond. Numerous studies of the adsorption of oxygen compounds on the surfaces of  $C_{60}$  fullerite powder and films [35,56–60] showed that at temperatures below 470 K water molecules from the air are physically adsorbed and remain on the surface even under high vacuum conditions. Since in our experiments, investigation was carried out at room temperature, most likely, there was a physical adsorption of water molecules. It was shown that when the samples are heated in a vacuum, some of the water molecules remain on the sample surface up to a temperature above 570 K, carbon oxides begin to form [35].

The XPS study of fullerite  $C_{60}$  [58,60] showed that the BE of O 1s electrons of water molecules adsorbed on the fullerite surface is in the 532–534 eV energy range and significantly less than that in a free  $H_2O$  molecule (535.75 eV) [61]. According to works [62–64], the BE of O 1s electrons of a water molecule, regardless of whether it is adsorbed on a metal, or metal oxide, lies in the BE range between 533 and 535 eV. The energy position of the O 1s signal of a water molecule adsorbed on the surface of a solid usually shifts down the BE scale as compared to a free molecule. This shift is usually attributed to surface screening effects since an inner shell vacancy in a water molecule is more effectively screened by

electrons on the surface than by those of a free water molecule. For a water molecule bound on a metal surface, two O 1s XPS peaks are commonly observed [64]. These peaks are associated with H<sub>2</sub>O (~532.5 eV) and hydroxyl groups (~531 eV) in the surface water layer, respectively. The presence of bound hydroxyl groups enhances water binding [61] because the H<sub>2</sub>O–OH H-bonding is stronger than the H<sub>2</sub>O–H<sub>2</sub>O H-bonding. For example, two O 1s XPS peaks at BE of 530.8 and 532.4 eV were observed for Cu(110) [61] and can clearly be resolved at 530.8–532.3 eV for Ru(0001) [65]. Moreover, the formation of a water bilayer was observed on the surface of metal [66], graphene [67] and fullerite C<sub>60</sub> [60] under ultra-high vacuum conditions. Thus, the comparison of our XPS results with those of other studies confirms the above interpretation that the low-energy component of the O 1s XPS spectrum of C<sub>60</sub> (532.2 eV) is associated with hydroxyl groups present in a surface water layer.

### 3.2. HIP-Treated Fullerite C<sub>60</sub> Study

At the first stage, the study of the structural transformation of fullerite C<sub>60</sub> during the HIP treatment was carried out by such traditional methods as XRD and Raman spectroscopy. The first method allows one to obtain the bulk structural characteristic of the condensed phase and its distortions in the transformation process as a whole, and the second characterizes the changes in the system states at the level of an individual molecular cluster of C<sub>60</sub>. However, these methods turn out to be of little information when it is necessary to analyze the C<sub>60</sub> molecule transformations and the formation of new stable carbon clusters. Therefore, the photoelectron and absorption X-ray spectroscopy was also used to characterize the structural changes in fullerite. The XPS and NEXAFS techniques make it possible to obtain the data on the nanoscale atomic structure of the sample and analyze the nearest surroundings and the charge state of an atom that absorbed an X-ray quantum. In other words, these methods also provide quantitative information on the local atomic and electronic structure of the sample.

Figure 2 shows the diffraction patterns of the pristine fullerite C<sub>60</sub> and four samples of fullerite C<sub>60</sub> HIP-treated at a pressure of 0.1 GPa and temperatures of 920, 1120, 1170 and 1270 K for 3 h in an Ar atmosphere. The stable phase of pure fullerite C<sub>60</sub> at atmospheric pressure and room temperature is the fcc one with the Fm3m spatial symmetry group. In the pristine C<sub>60</sub> XRD pattern, the characteristic features of the fullerite C<sub>60</sub> fcc phase the (200) and (400) diffraction peaks are missing due to C<sub>60</sub> molecule rapid rotation at atmospheric pressure and room temperature. The characteristic features of the X-ray diffraction pattern of the fullerite C<sub>60</sub> fcc phase are the (200) and (400) diffraction peaks missing at atmospheric pressure and room temperature due to C<sub>60</sub> molecule rapid rotation. With increasing temperature, strong structural changes in diffractograms due to the transition from the fcc molecular crystal to an amorphous solid-state phase are observed. A series of clear narrow peaks in the region  $2\theta = 10\text{--}24^\circ$  in the fcc diffraction pattern of the fullerite C<sub>60</sub> phase shows that the starting material is a molecular crystal with a high degree of perfection. On the diffractograms at a 920 K temperature there is no shift, broadening and splitting of these diffraction peaks. This suggests that the C<sub>60</sub> cluster remains the main structural unit of the system and, at the same time, there is no change in the distances between fullerene molecules. However, a noticeable change in the relative intensities of the diffraction lines and the appearance of weak additional reflexes in the region of large diffraction angles of  $40\text{--}50^\circ$  are observed, which indicates a distortion of the structure of the initial crystalline phase structure and the beginning of the process of forming a chemical bond between C<sub>60</sub> molecules.

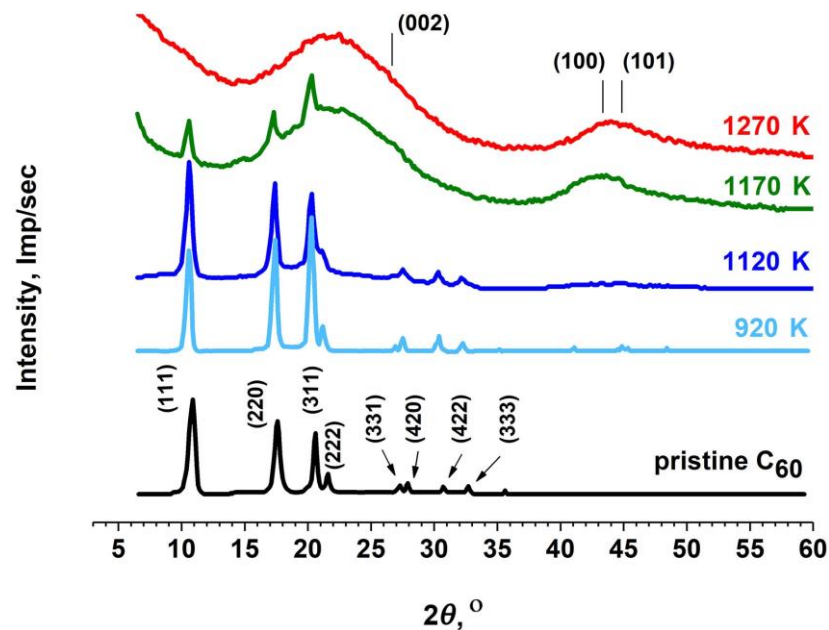


**Figure 2.** XRD patterns of the pristine and HIP-treated at different temperatures fullerite  $C_{60}$ . The vertical lines at the top indicate the HOPG diffraction peaks (002), (100) and (101).

With a further increase in temperature to 1120 K, a slight broadening of the main diffraction peaks is observed, indicating the formation of covalent C–C bonds and a change in the distances between the molecules. The appearance of two wide-diffuse lines located in the 15–30° and 40–50° regions on diffractograms is the beginning of the  $C_{60}$  cluster destruction. When the temperature rises to 1170 K, the destruction increases, and at 1270 K the diffraction lines in the angle range of 10–24°, characteristic of the molecular cluster, disappear and two wide lines at angles of ~22° and ~44° are observed. The obtained data demonstrate that the limit of the cluster  $C_{60}$  thermal stability at a pressure of 0.1 GPa is ~1000 K and corresponds to the thermal stability limit of the  $C_{60}$  fullerene molecule at atmospheric pressure [68]. The diffraction patterns of the fullerite sample at a temperature of 1270 K are qualitatively similar to the ones of the materials formed at the carbonization final stages and graphitization initial stages of various carbon-containing compounds [69–73]. Their diffraction patterns are also characterized by the presence of several wide diffuse lines.

The diffuse band appearance at 41–47°, corresponding to two-dimensional (10) and (11) graphene layer reflexes and (100) and (101) HOPG peaks, indicates the presence of a small amount of graphene layer fragments with various degrees of defectiveness in the system [69,70]. A wide band in the region of 20–30° is characterized by a maximum, the position of which approximately corresponds to that of the (002) diffraction peak of graphite and MWCNTs. This indicates that a significant number of these two-dimensional ordered carbon clusters is a part of crystallites from packages of nanoscale graphene layers [69,70]. However, it should be noted that the absence of three-dimensional (hkl) reflexes on the diffractograms indicates the absence of a three-dimensional ordering of graphene planes characteristic of graphite. The estimation of the average sizes of nanoparticles using the Warren–Scherrer equation [69,74], which relates the average lateral dimensions  $L_a$  and the height (thickness)  $L_c$  of the graphene layers packaging with the width of the corresponding (10), (11) and (002) diffraction peaks, showed that the average values of the  $L_a$  and  $L_c$  parameters were in the range 2–4 nm.

A similar sequence of changes in the fullerite structure can be traced on the basis of the temperature dependence of the Raman spectra shown in Figure 3. The  $C_{60}$  Raman spectra change slightly with an increase in the temperature up to 1120 K. All the above-mentioned spectra preserve the pristine  $C_{60}$  spectrum main features, even though they

show a small broadening and a decrease in peak intensities over the entire spectral range except the 1200–1800  $\text{cm}^{-1}$  region where the wide band formation is observed. However, at temperatures above 1120 K, the Raman spectra change significantly, especially in the 1100–1700  $\text{cm}^{-1}$  region. In particular, the intensities of the all peaks decrease and a wide band in the 2600–3200  $\text{cm}^{-1}$  region appears. Moreover, one can see a very low-intensity peak at 96  $\text{cm}^{-1}$ , strong decrease in intensity and red shift of the “pentagonal pinch” mode from 1468  $\text{cm}^{-1}$  to 1462  $\text{cm}^{-1}$ . A new peak appearing in the Raman spectrum of  $\text{C}_{60}$  at 96  $\text{cm}^{-1}$  and the red shift of the  $A_g(2)$  “pentagonal pinch” mode indicate the formation of dimers of the  $\text{C}_{60}$  molecule in a fullerite during the HIP treatment. At the same time, according to the XRD data (Figure 2), the pristine fullerite fcc structure was partially preserved. The appearance of a low-energy peak (96  $\text{cm}^{-1}$ ) is caused by a full-symmetric oscillation of the  $\text{C}_{60}$  molecules in the dimer. The frequency of this oscillation is in good agreement with its theoretically predicted value [75], which is also confirmed experimentally [76,77]. Moreover, the  $A_g(2)$  “pentagonal pinch” mode (1463  $\text{cm}^{-1}$ ) is associated with the  $A_g(2)$  mode for the  $\text{C}_{60}$  dimer [78]. Instead of narrow peaks  $H_g(6)$ – $H_g(8)$  two very broad bands at 1350  $\text{cm}^{-1}$  and 1591  $\text{cm}^{-1}$  appear. The intensity of these bands grows with the increasing temperature up to 1270 K. As a result, all the pristine  $\text{C}_{60}$  features in the Raman shift spectrum disappear, which indicates the complete destruction of the  $\text{C}_{60}$  molecules. The absence of the  $A_g(2)$  “pentagonal pinch” mode, as well as the appearance of the “graphitic” G-band and disorder-induced D-band in the Raman spectrum, on the one hand, indicates the complete destruction of pentagonal rings, and on the other hand, the formation of nanoscale structures consisting of hexagonal rings.

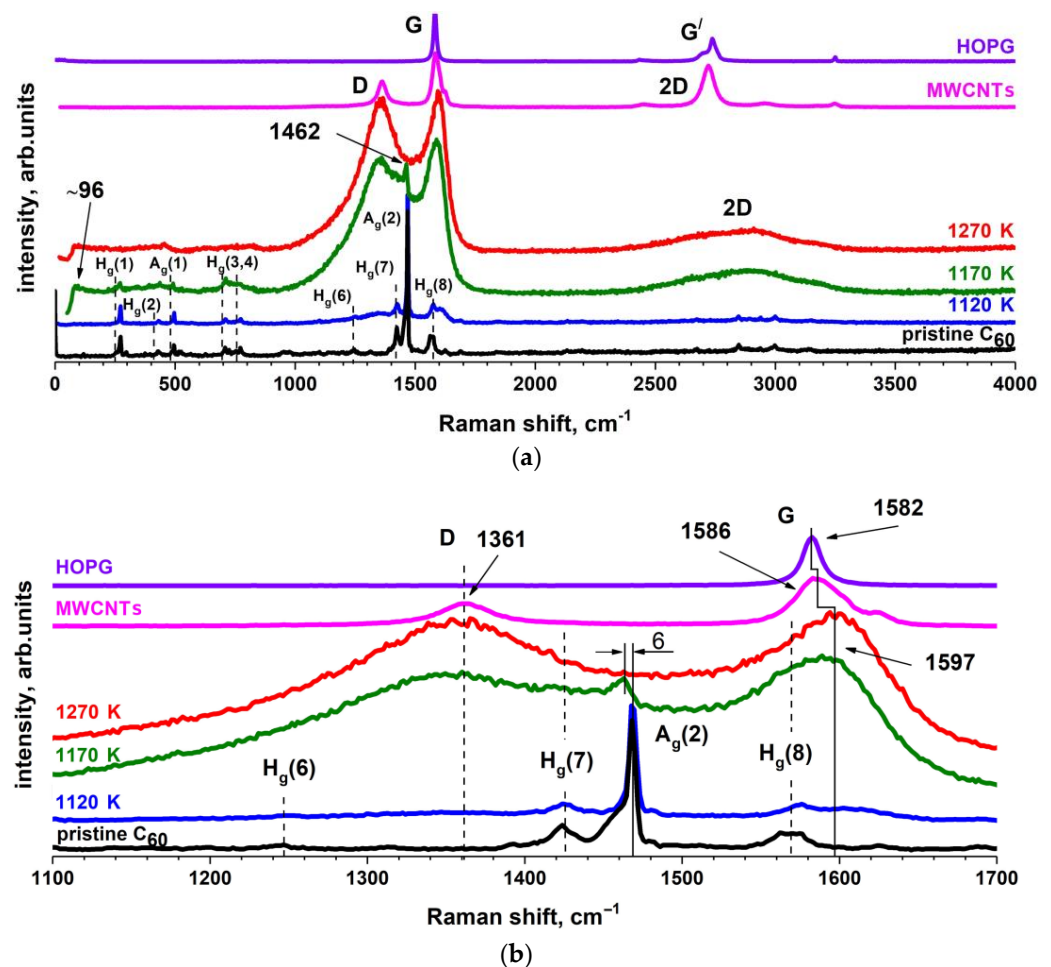


**Figure 3.** Raman spectra of the HOPG, MWCNTs, pristine and HIP-treated at different temperatures fullerite  $\text{C}_{60}$  over a wide spectral range (a) and in the region of 1100–1700  $\text{cm}^{-1}$  (b).



Figure 3 shows that the spectra of the modified fullerite have significantly widened G, D and 2D bands. A comparison of the Raman spectrum of the fullerite  $C_{60}$  with those of HOPG and MWCNTs (Figure 3b) shows that the energy position of the D band of  $C_{60}$  is consistent with its position in the HOPG and MWCNTs spectra, while the position of the G band ( $1597\text{ cm}^{-1}$ ) undergoes a low energy shift of  $11\text{ cm}^{-1}$  for MWCNTs ( $1586\text{ cm}^{-1}$ ) and  $15\text{ cm}^{-1}$  for HOPG ( $1582\text{ cm}^{-1}$ ). An essential point is the absence of narrow 2D peaks in the range of  $2300\text{--}3200\text{ cm}^{-1}$  in the spectrum of the HIP-treated  $C_{60}$ , and only a weakly modulated very wide band is present. The absence of peaks in the  $2300\text{--}3200\text{ cm}^{-1}$  region of Raman spectra in the three-stage model of classification of the graphite disorderliness degree during the transition from graphite to amorphous carbon [49] suggests that fullerite  $C_{60}$  after HIP treatment is an intermediate material between the first (nanocrystalline graphite) and the second (mainly  $sp^2$  or low  $sp^3$  amorphous carbon) stages.

The dimensions of this material structural elements can be estimated using an empirical relation between the intensity (area) ratios of the G and D bands and the average sizes of crystallites or large molecules  $L_a$  [49,79] as  $I(D)/I(G) = C(\lambda)/L_a$ , where  $C(\lambda)$  is a constant that depends on the laser radiation wavelength  $\lambda$  and is equal to  $4.4\text{ nm}$  for  $\lambda = 488\text{ nm}$ . In our case,  $L_a \approx 2.5\text{ nm}$ , which is quite comparable to the fullerene  $C_{60}$  molecule diameter ( $\sim 1\text{ nm}$ ) and is consistent with the X-ray phase analysis data ( $\sim 2\text{--}4\text{ nm}$ ). It is known that with a certain orientation of two neighboring  $C_{60}$  molecules, when the double bonds are parallel to each other, polymerization processes of  $C_{60}$  fullerene molecules by the [2+2]-cycloaddition reaction are possible [4,5,80,81]. In the work [81], it was shown that by 23 consecutive turns of bonds, or the so-called generalized Stone–Wales (GSW) transformations, it is possible to describe the fusion of two fullerene  $C_{60}$  molecules into a  $C_{120}$  nanocapsule (a short nanotube  $2\text{--}3\text{ nm}$  long) with the surface consisting mainly of hexagons.

It should be noted that in the solid state, a fullerene  $C_{60}$  molecule can interact by the [2+2]-cycloaddition reaction with at least four neighboring molecules. Given the size of the fullerene molecule, it is possible that two competing transformation processes occur simultaneously. This can lead to a sharp increase of the GSW transformation activation energy barrier and to the fusion process termination. Studies on modeling the molecular transformation of two fullerene  $C_{60}$  molecules into a  $C_{120}$  nanocapsule were carried out in the work [4]. Authors found that, depending on the initial orientation of the molecules,  $C_{120}$  nanocapsules of different chirality with diameters in the range of  $0.68\text{--}0.98\text{ nm}$  can be formed.

The fusion of fullerene molecules into a cylindrical structure during heating to temperatures above  $1370\text{ K}$  in a vacuum was observed experimentally by transmission electron microscopy [6]. In this study, fullerene molecules located inside single-walled nanotubes were used. In the works [7,82], high-resolution transmission electron microscopy (HRTEM) was used to study HIP-treated fullerite  $C_{60}$  at a pressure of  $0.15\text{ GPa}$  and temperature of  $1300\text{ K}$  in nitrogen [7], and at  $0.22\text{ GPa}$  and  $1670\text{ K}$  in argon [82]. In these studies, it was shown that the structure of the fullerite  $C_{60}$  after HIP treatment is a disoriented sequence of curved fragments with a size of  $\sim 1\text{--}5\text{ nm}$ . In the work [8], a similar picture of HRTEM images of randomly oriented graphite-type clusters with sizes of  $1.5\text{--}3\text{ nm}$ , synthesized from fullerite  $C_{60}$  at a temperature of  $1270\text{ K}$  and a pressure in the range of  $1.5\text{--}8\text{ GPa}$  were obtained.

In order to clarify the symmetry and composition of the carbon atom's nearest environment in the HIP-modified fullerite  $C_{60}$  samples, the NEXAFS spectroscopy was used. Figure 4 shows the C 1s NEXAFS spectra of the pristine and HIP-treated fullerite  $C_{60}$ , obtained after subtracting the contribution to the absorption of the overlying shells and normalized to the absorption level at the photon energy of  $320\text{ eV}$ . The spectrum of  $C_{60}$  HIP-treated at a temperature of  $920\text{ K}$  contains all the peaks characteristic of the pristine fullerite. However, there is a significant decrease in the intensity of the first peak and a change in the relative intensities of the first three absorption bands, which correspond to transitions to the unoccupied antibonding  $\pi^*$ -orbitals of the  $C_{60}$  molecule. This is in good

agreement with the XRD and Raman spectroscopy data and demonstrates that fullerene molecules retain their structure. In the work [83], similar changes in C 1s NEXAFS spectrum of C<sub>60</sub> powder after treatment at a pressure of 1.1–1.2 GPa and a temperature of 580–585 K were observed and interpreted as the evidence of the formation of covalent C–C bonds and changes in the distances between C<sub>60</sub> molecules.

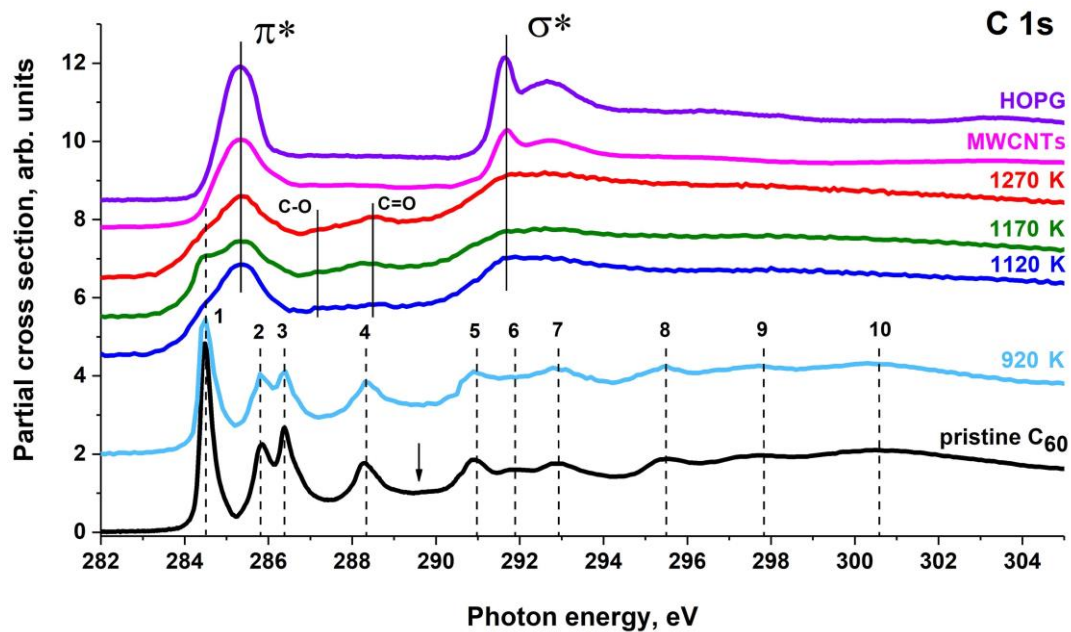


**Figure 4.** C 1s NEXAFS spectra of the HOPG, MWCNTs, pristine and HIP-treated at different temperatures fullerite C<sub>60</sub>. The arrow indicates the position of the fullerite C<sub>60</sub> C 1s absorption edge (289.60 eV) [42]. The HOPG spectrum was obtained at the 40° grazing incidence angle of a linearly polarized SR beam on the sample surface.

With an increase in temperature to 1170 K and further to 1270 K, C 1s NEXAFS spectrum is dramatically changed, as in the cases of the XRD patterns and Raman spectra. In particular, all the peaks present in the C 1s NEXAFS spectrum of the pristine C<sub>60</sub> disappear, with the exception of the first intense peak, which is transformed into a shoulder on the low-energy side of the new absorption band at photon energy of 285.4 eV. In addition, new absorption structures appeared in the spectrum: a broad band at an energy of 291.7 eV, and two low-intensity bands at 287.2 eV and 288.9 eV, corresponding to C1s  $\rightarrow \pi^*$  transitions in the C–O and C=O groups [43]. At a temperature of 1270 K, the absorption structure characteristic of the C 1s NEXAFS spectrum of the C<sub>60</sub> fullerene molecule disappears, thus indicating the complete destruction of the C<sub>60</sub> molecule and the formation of a new material. The absorption bands of the C 1s NEXAFS spectrum of this new material correlate well with the ones in the corresponding spectra of HOPG and MWCNTs. This means that the nearest environment of the carbon atom corresponds to a hexagonal graphene network of a high degree of perfection. In the case of nanoparticles with a size of 2–5 nm, the occurrence of such an atomic environment is possible if these particles have closed graphene surfaces. The formation of such structures during HIP treatment is predicted theoretically from C<sub>60</sub> dimers and confirmed experimentally [4,5,20,81]. In our case, the C<sub>60</sub> dimer formation is confirmed by the Raman spectra analysis.

In the NEXAFS spectrum of C<sub>60</sub> powder after HIP treatment at 1120 K (Figure 4), there are two bands associated with carbon-oxygen groups, the intensities of which are enhanced with the treatment temperature increasing. The reason for the appearance of these bands is the interaction with molecular water, which was adsorbed on the pristine C<sub>60</sub> powder surface. As discussed earlier in Section 3.1, the formation of carbon oxides [35] occurs already at 570 K, but the corresponding peaks in the sample C 1s NEXAFS spectrum of the sample at 920 K are not observed.

The comparison between the C 1s NEXAFS spectra of pristine HOPG and MWCNTs, and C<sub>60</sub> powder HIP treated at a temperature of 1270 K (Figure 5a) clearly demonstrates the sequential broadening of the first  $\pi^*$  peak during going from the HOPG spectrum to the MWCNTs one and then to the HIP-treated sample spectrum. The main reason of these spectral changes is an increase in distortions, which is clearly visible from the changes in the width and intensity of the D band in the Raman spectra presented in Figure 3. This band broadening may occur due to the formation of carbon oxides during HIP treatment. To find this out the C 1s NEXAFS spectral studies of MWCNTs after HIP treatment under the same conditions were conducted. In this study the atomic oxygen content in the initial sample was about 4%, the same as one on the surface of the pristine C<sub>60</sub> powder.

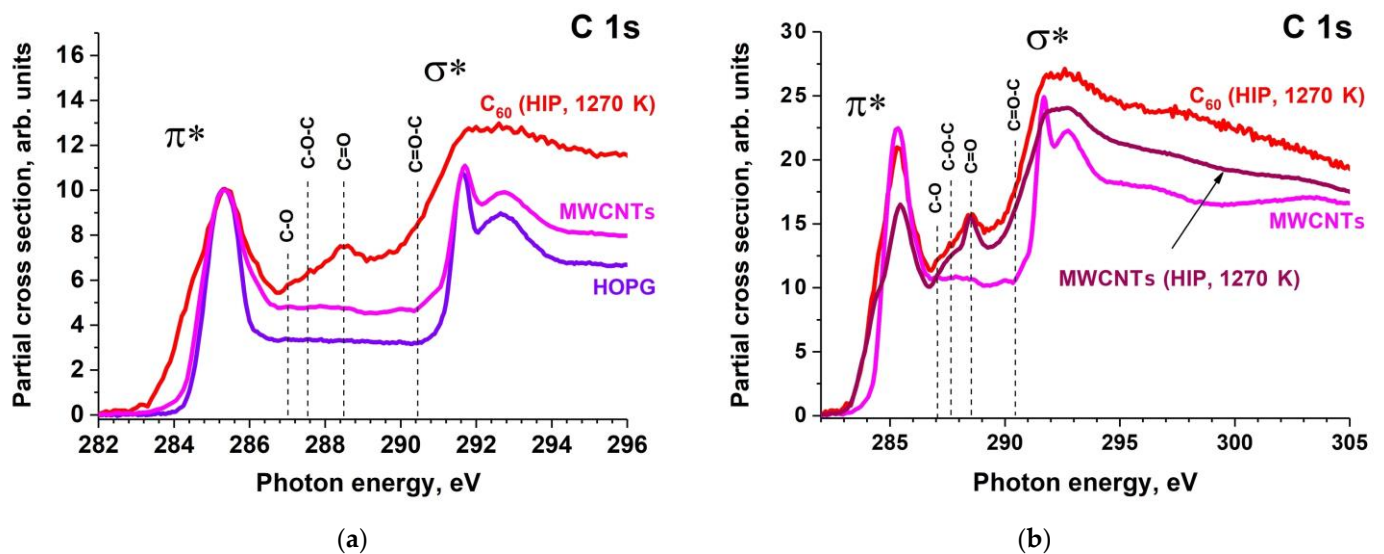


**Figure 5.** C 1s NEXAFS spectra of HOPG, MWCNTs and fullerite C<sub>60</sub> HIP-treated at 1270 K, (a) normalized the  $\pi^*$  peak maximum and (b) normalized to the photoabsorption cross section at the photon energy of 320 eV.

Figure 5b shows the C 1s NEXAFS spectrum of the pristine MWCNTs, and HIP-treated C<sub>60</sub> powder and MWCNTs. The treatment was performed in an argon atmosphere at pressure of 0.1 GPa and temperature of 1270 K for 3 hours. The figure demonstrates the broadening of the  $\pi^*$  and  $\sigma^*$  absorption bands and the appearance of the peaks characteristic of the C–O, C–O–C, O=C–O and C=O functional groups in the HIP-treated MWCNTs C 1s NEXAFS spectrum. This confirms that the broadening of the absorption bands is caused by the formation of carbon oxides during the C<sub>60</sub> HIP treatment. Taking into account the impossibility of the complete removal of adsorbed water even in a high vacuum, it is very likely to expect the appearance of the absorption bands associated with the presence of carbon oxides in the C 1s NEXAFS spectrum of the carbon material subjected to HIP treatment in inert media.

The high sensitivity of the C 1s NEXAFS spectrum of the new carbon material to the presence of the C–O, C–O–C, O=C–O and C=O functional groups is due to the high oscillator strengths of C1s  $\rightarrow \pi^*$  transitions in such linear atomic groups. Therefore, even at small oxide concentrations, their presence is manifested in C 1s NEXAFS spectra. To determine the quantitative atomic concentration of oxygen in the fullerite C<sub>60</sub> powder after HIP treatment at 1270 K, its C 1s XPS spectra were measured. The overview XPS spectrum of the C<sub>60</sub> powder after HIP treatment at 1270 K (Figure 6) contains a C 1s peak at 284.7 eV (FWHM is 1.4) and a broad O 1s line at 532.7 eV (FWHM is 2.6). The XPS measurements allow the determination of the relative atomic concentration of oxygen on the HIP-treated powder C<sub>60</sub> surface equal to 4%. The O 1s peak in the XPS spectra indicates the presence of oxygen-containing compounds on the sample surface (carbon oxides as well as water and oxygen molecules physically adsorbed from the atmosphere).

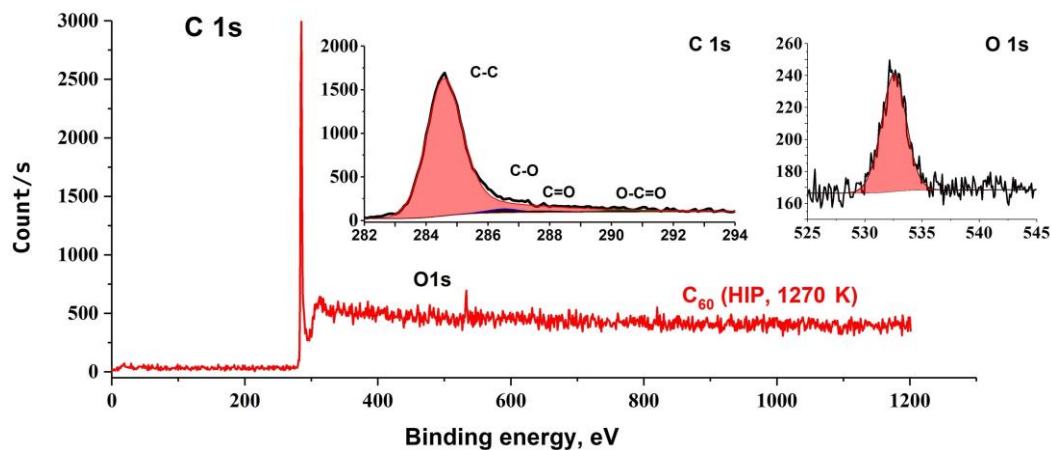


**Figure 6.** Survey XPS spectra of the fullerite  $C_{60}$  subjected to HIP treatment at 1270 K and subsequently exposed to air for a long time. The insets show C 1s and O 1s core-level XPS spectra.

As can be seen from the C 1s core-level PE spectrum (left inset in Figure 6) the main C 1s peak is asymmetric and splits into four components at the BE of 284.7 eV (C–C), 286.5 eV (C–O), 287.6 eV (C=O) and  $\sim 290$  eV (O=C–O). The O 1s peak (right inset in Figure 6) is symmetric and the separation of O 1s signals associated with different oxygen-containing groups and adsorbed water molecules is not possible. From a comparison of the peak areas of the C 1s and O 1s XPS spectra of the  $C_{60}$  powder treated with HIP, it was found that the ratio of the number of oxygen atoms participating in the formation of oxygen-containing groups and the adsorption of water molecules on the sample surface to the number of carbon atoms, is about of 3%. The presence of a broad band at a BE of  $\sim 290$  eV in C 1s XPS spectrum explains the appearance of a wide shoulder at the low-energy side of the  $\sigma^*$  absorption band in C 1s NEXAFS spectrum of the MWCNTs and HIP-treated fullerite (Figure 6) as the contribution of C1s  $\rightarrow \pi^*$  transitions in the O=C–O group [43].

The analysis of the XPS and NEXAFS spectroscopy data suggests that with an increase in temperature during the HIP treatment, the destruction of the fullerite  $C_{60}$  molecular structure occurs with the formation of  $C_{60}$  dimers at a temperature of 1170 K, as well as the fusion of fullerene molecules into nanocapsules with a graphene surface and the formation of a new material at a temperature of 1270 K. A comparison between the C 1s NEXAFS spectra of this material and MWCNTs allows to assert that the obtained material is not a disoriented graphite phase, but a set of arbitrary oriented closed graphene surfaces connected with covalent bond, in which carbon atoms have the high environment stoichiometry as in graphene.

#### 4. Conclusions

The  $C_{60}$  powder samples subjected to HIP treatment were studied by a complementary set of methods (XRD, XPS, NEXAFS and Raman spectroscopy). The obtained results were analyzed using a literature data on electron microscopy [7,8,82] and various theoretical approaches [4,5,80,81]. The conducted study clearly shows the advantages of combining different complementary theoretical and experimental methods for the most complete characterization of such complex samples. A strong bonding of the water molecules with the  $C_{60}$  powder, MWCNTs and the surface of the HOPG was found. Using the XPS method, the presence of a residual surface layer of water molecules on all samples even under ultrahigh vacuum was detected and the concentration of oxygen atoms was determined as equal to 4–8%. Thus, the presence of adsorbed water on the surface of fullerite and MWCNTs leads to the formation of carbon oxides during HIP treatment, with the concentration of carbon atoms bonded with oxygen atoms equals to  $\sim 3\%$ .

The analysis of the data obtained by a complementary set of methods showed the following scenario of the pristine fullerite  $C_{60}$  powder transformation into closed graphene



shells of 2–5 nm in size, connected by covalent bonds. At the first stage of HIP treatment, when heated to a temperature of 920 K, fullerite retains its crystalline fcc structure, but the process of forming bonds between molecules and the formation of C<sub>60</sub> dimers begins. This is expressed in a decrease and change in the relative intensity of the first four bands in the C 1s NEXAFS spectrum. With an increase in temperature to 1120 K, the process of bond formation becomes more intense, which is evident from the presence of peaks characteristic of C<sub>60</sub> dimers in the Raman spectra and the preservation of the fcc structure reflexes on the diffractogram. However, at the same time, the process of merging neighboring molecules begins, which ends at 1270 K with the transformation of fullerene molecules into capsules of 2–5 nm in size. These capsules are completely disoriented, which is clearly seen by the appearance of diffuse bands on diffractograms and Raman spectra, and is confirmed by HRTEM data [7,8,82]. The mechanism of such capsule formation through the fusion of C<sub>60</sub> fullerene molecules during HIP treatment is predicted theoretically and described in detail in the work [81], but has no experimental confirmation. To solve this problem, it is necessary to show the formation of a closed graphene surface during fullerite HIP treatment. The proof can be the formation of the carbon atom environment after HIP treatment, similar to one in the case of HOPG or pure MWCNTs.

The best method for solving this problem is NEXAFS spectroscopy. In the modern publications, there is no data on the study of HIP-treated fullerite C<sub>60</sub> by spectroscopy methods. In the paper, for the first time, systematic studies of HIP-treated fullerite C<sub>60</sub> with a sequential step-by-step increase in temperature were carried out by a complementary set of methods, including XPS and NEXAFS spectroscopy using synchrotron radiation. Successive changes in the C<sub>60</sub> powder subjected to HIP treatment at temperatures equal to 920, 1120, 1170 and 1270 K clearly demonstrate the formation of a structure in the form of  $\pi^*$  and  $\sigma^*$  absorption bands in the C<sub>60</sub> powder C 1s NEXAFS spectrum, also presented in the C 1s NEXAFS spectra of HOPG, MWCNTs and MWCNTs HIP-treated at a temperature of 1270 K. Nanoparticles of 2–5 nm in size stacked in several graphene-like layers cannot be characterized by an ideal arrangement of carbon atoms, as in the case of HOPG and MWCNTs, except for the case when they form a closed surface consisting of hexagons.

Thus, the conducted studies have shown that using HIP treatment of fullerite C<sub>60</sub> powder at a temperature of 1270 K and a pressure of 0.1 GPa in an argon atmosphere, a chemical resistant material with high hardness and elasticity at a density lower than graphite consisting of closed graphene surfaces with a size of 2–5 nm connected by covalent bonds can be obtained. This material is promising for various applications and as a basis for the synthesis of new composite materials.

**Author Contributions:** Conceptualization, D.V.S. and O.V.P.; research supervision, D.V.S., O.V.P., S.V.N. and V.N.S.; writing—original draft, D.V.S., O.V.P., S.V.N., A.S.V. and V.N.S.; fullerite C<sub>60</sub> HIP treatment, XRD measurement and its data interpretation, A.M.O. and B.S.K.; Raman spectroscopy measurements, S.I.I.; XPS and NEXAFS spectroscopy measurements and their data analysis, D.V.S., O.V.P., S.V.N., A.S.V., R.N.S., K.A.B. and V.N.S. All the authors discussed the results and commented on the manuscript during its preparation. All authors have read and agreed to the published version of the manuscript.

**Funding:** The reported study was funded by RFBR, project number 19-32-60018, and the Komi Republic within the framework of research project No. 20-42-110002 r-a, the Grant of the President of the Russian Federation (MK-3796.2021.1.2), the bilateral program of the Russian–German laboratory at BESSY II and the state research target for the G.A. Razuvaev Institute of Organometallic Chemistry of RAS (theme No. 45.4). The study was supported by the Ministry of Science and Higher Education of Russia under Agreement N 075-15-2021-1351 in part of research on NEXAFS spectroscopy. The work was carried out using the equipment of the center for collective use “Analytical Center of the IOMC RAS” with the financial support of the grant “Ensuring the development of the material and technical infrastructure of the centers for collective use of scientific equipment” (Unique identifier RF—2296.61321X0017, Agreement Number 075-15-2021-670).

**Institutional Review Board Statement:** Not applicable.

**Acknowledgments:** Scientific research were performed at the Center for Studies in Surface Science of Research Park of St. Petersburg State University, and the Center for Collective Use at the Institute of Geology of Komi Science Centre of the Ural Branch of RAS.

**Conflicts of Interest:** The authors declare no conflict of interest. The funders had no role in the design of the study; in the collection, analyses, or interpretation of data; in the writing of the manuscript, or in the decision to publish the results.

## References

1. Krättschmer, W.; Lamb, L.D.; Fostiropoulos, K.; Huffman, D.R. Solid C<sub>60</sub>: A new form of carbon. *Nature* **1990**, *347*, 354–358. [[CrossRef](#)]
2. Howard, J.B.; McKinnon, J.T.; Makarovskiy, Y.; Lafleur, A.L.; Johnson, M.E. Fullerenes C<sub>60</sub> and C<sub>70</sub> in flames. *Nature* **1991**, *352*, 139–141. [[CrossRef](#)] [[PubMed](#)]
3. Lieber, C.M.; Chen, C.C. Preparation of fullerenes and fullerene based materials. In *Solid State Physics*; Ehrenreich, H., Spaepen, F., Eds.; Academic Press: New York, NY, USA, 1994; Volume 48, pp. 109–148.
4. Kim, Y.-H.; Lee, I.-H.; Chang, K.J.; Lee, S. Dynamics of fullerene coalescence. *Phys. Rev. Lett.* **2003**, *90*, 065501. [[CrossRef](#)]
5. Stafström, S.; Fagerström, J. Electronic structure and stability of fullerene polymers. *Appl. Phys. A Mater. Sci. Process.* **1997**, *64*, 307–314. [[CrossRef](#)]
6. Bandow, S.; Takizawa, M.; Hirahara, K.; Yudasaka, M.; Iijima, S. Raman scattering study of double-wall carbon nanotubes derived from the chains of fullerenes in single-wall carbon nanotubes. *Chem. Phys. Lett.* **2001**, *337*, 48–54. [[CrossRef](#)]
7. Brazhkin, V.V.; Lyapin, A.G.; Solozhenko, V.L.; Bugakov, V.I.; Dub, S.N.; Kurakevych, O.O.; Kondrin, M.V.; Gromnitskaya, E.L. High-temperature transitions of C<sub>60</sub> at moderate pressures. *Fuller. Nanotub. Carbon Nanostruct.* **2008**, *16*, 475–485. [[CrossRef](#)]
8. Tat'yanin, E.V.; Lyapin, A.G.; Mukhamadiarov, V.V.; Brazhkin, V.V.; Vasiliev, A.L. Mechanism of formation of the superhard disordered graphite-like phase from fullerite C<sub>60</sub> under pressure. *J. Phys. Condens. Matter* **2005**, *17*, 249–256. [[CrossRef](#)]
9. Duclos, S.J.; Brister, K.; Haddon, R.C.; Kortan, A.R.; Thiel, F.A. Effects of pressure and stress on C<sub>60</sub> fullerite to 20 GPa. *Nature* **1991**, *351*, 380–382. [[CrossRef](#)]
10. Samara, G.A.; Schirber, J.E.; Morosin, B.; Hansen, L.V.; Loy, D.; Sylwester, A.P. Pressure dependence of the orientational ordering in solid C<sub>60</sub>. *Phys. Rev. Lett.* **1991**, *67*, 3136–3139. [[CrossRef](#)] [[PubMed](#)]
11. Yoo, C.S.; Nellis, W.J. Phase transformations in carbon fullerenes at high shock pressures. *Science* **1991**, *254*, 1489–1491. [[CrossRef](#)]
12. Kriza, G.; Ameline, J.-C.; Jérôme, D.; Dworkin, A.; Szwarc, H.; Fabre, C.; Schütz, D.; Rassat, A.; Bernier, P.; Zahab, A. Pressure dependence of the structural phase transition in C<sub>60</sub>. *J. Phys. I Fr.* **1991**, *1*, 1361–1364. [[CrossRef](#)]
13. Yoo, C.S.; Nellis, W.J. Phase transition from C<sub>60</sub> molecules to strongly interacting C<sub>60</sub> agglomerates at hydrostatic high pressures. *Chem. Phys. Lett.* **1992**, *198*, 379–382. [[CrossRef](#)]
14. Moshary, F.; Chen, N.H.; Silvera, I.F.; Brown, C.A.; Dorn, H.C.; de Vries, M.S.; Bethune, D.S. Gap reduction and the collapse of solid C<sub>60</sub> to a new phase of carbon under pressure. *Phys. Rev. Lett.* **1992**, *69*, 466–469. [[CrossRef](#)] [[PubMed](#)]
15. Yamawaki, H.; Yoshida, M.; Kakudate, Y.; Usuba, S.; Yokoi, H.; Fujiwara, S.; Aoki, K.; Ruoff, R.; Malhotra, R.; Lorents, D. Infrared study of vibrational property and polymerization of fullerene C<sub>60</sub> and C<sub>70</sub> under pressure. *J. Phys. Chem.* **1993**, *97*, 11161–11163. [[CrossRef](#)]
16. Bashkin, I.O.; Rashchupkin, V.I.; Gurov, A.F.; Moravskiy, A.P.; Rybchenkot, O.G.; Kobelev, N.P.; Soifer, Y.M.; Ponyatovskiy, E.G. A new phase transition in the T-P diagram of C<sub>60</sub> fullerite. *J. Phys. Condens. Matter* **1994**, *6*, 7491–7498. [[CrossRef](#)]
17. Iwasa, Y.; Arima, T.; Fleming, R.M.; Siegrist, T.; Zhou, O.; Haddon, R.C.; Rothberg, L.J.; Lyons, K.B.; Carter, H.L.; Hebard, A.F.; et al. New phases of C<sub>60</sub> synthesized at high pressure. *Science* **1994**, *264*, 1570–1572. [[CrossRef](#)]
18. Núñez-Regueiro, M.; Marques, L.; Hodeau, J.-L.; Béthoux, O.; Perroux, M. Polymerized fullerite structures. *Phys. Rev. Lett.* **1995**, *74*, 278–281. [[CrossRef](#)]
19. Blank, V.; Popov, M.; Buga, S.; Davydov, V.; Denisov, V.N.; Ivlev, A.N.; Marvin, B.N.; Agafonov, V.; Ceolin, R.; Szwarc, H.; et al. Is C<sub>60</sub> fullerite harder than diamond? *Phys. Lett. A* **1994**, *188*, 281–286. [[CrossRef](#)]
20. Sundqvist, B. Fullerenes under high pressures. *Adv. Phys.* **1999**, *48*, 1–134. [[CrossRef](#)]
21. Blank, V.D.; Buga, S.G.; Dubitsky, G.A.; Serebryanaya, N.R.; Popov, M.Y.; Sundqvist, B. High-pressure polymerized phases of C<sub>60</sub>. *Carbon* **1998**, *36*, 319–343. [[CrossRef](#)]
22. Brazhkin, V.V.; Lyapin, A.G.; Popova, S.V.; Bayliss, S.C.; Varfolomeeva, T.D.; Voloshin, R.N.; Gavrilyuk, A.G.; Kondrin, M.V.; Mukhamad'yarov, V.V.; Troyan, I.A.; et al. Interplay between the structure and properties of new metastable carbon phases obtained under high pressures from fullerite C<sub>60</sub> and carbyne. *J. Exp. Theor. Phys. Lett.* **2002**, *76*, 681–692. [[CrossRef](#)]
23. Wood, R.A.; Lewis, M.H.; West, G.; Bennington, S.M.; Cain, M.G.; Kitamura, N. Transmission electron microscopy, electron diffraction and hardness studies of high-pressure and high-temperature treated C<sub>60</sub>. *J. Phys. Condens. Matter* **2000**, *12*, 10411–10421. [[CrossRef](#)]
24. Gadd, G.E.; Moricca, S.; Kennedy, S.J.; Elcombe, M.M.; Evans, P.J.; Blackford, M.; Cassidy, D.; Howard, C.J.; Prasad, P.; Hanna, J.V.; et al. Novel rare gas interstitial fullerenes of C<sub>60</sub> with Ar, Kr and Xe. *J. Phys. Chem. Solids* **1997**, *58*, 1823–1832. [[CrossRef](#)]
25. Shul'ga, Y.M.; Martynenko, V.M.; Polyakov, S.N.; Chelovskaya, N.V.; Open'ko, V.V.; Skokan, E.V.; Blinova, L.N.; Dobrovolskii, Y.A.; Morozov, Y.G.; Razumov, V.F.; et al. Fullerite intercalated with argon at room temperature: Synthesis and physicochemical properties. *Russ. J. Inorg. Chem.* **2009**, *54*, 341–345. [[CrossRef](#)]

26. Stöhr, J. *NEXAFS Spectroscopy*; Springer Series in Surface Sciences; Springer: Berlin/Heidelberg, Germany, 1992; Volume 25, ISBN 978-3-642-08113-2.
27. Hüfner, S. *Photoelectron Spectroscopy*; Advanced Texts in Physics; Springer: Berlin/Heidelberg, Germany, 2003; ISBN 978-3-642-07520-9.
28. Hofmann, S. *Auger- and X-ray Photoelectron Spectroscopy in Materials Science*; Springer Series in Surface Sciences; Springer: Berlin/Heidelberg, Germany, 2013; Volume 49, ISBN 978-3-642-27380-3.
29. Sivkov, D.; Petrova, O.; Mingaleva, A.; Ob'edkov, A.; Kaverin, B.; Gusev, S.; Vilkov, I.; Isaenko, S.; Bogachuk, D.; Skandakov, R.; et al. The structure and chemical composition of the Cr and Fe pyrolytic coatings on the MWCNTs' surface according to NEXAFS and XPS spectroscopy. *Nanomaterials* **2020**, *10*, 374. [[CrossRef](#)] [[PubMed](#)]
30. Sivkov, D.; Nekipelov, S.; Petrova, O.; Vinogradov, A.; Mingaleva, A.; Isaenko, S.; Makarov, P.; Ob'edkov, A.; Kaverin, B.; Gusev, S.; et al. Studies of buried layers and interfaces of tungsten carbide coatings on the MWCNT surface by XPS and NEXAFS spectroscopy. *Appl. Sci.* **2020**, *10*, 4736. [[CrossRef](#)]
31. Gorovikov, S.A.; Molodtsov, S.L.; Follath, R. Optical design of the high-energy resolution beamline at a dipole magnet of BESSY II. *Nucl. Instrum. Methods Phys. Res. Sect. A Accel. Spectrometers Detect. Assoc. Equip.* **1998**, *411*, 506–512. [[CrossRef](#)]
32. Fedoseenko, S.I.; Vyalikh, D.V.; Iossifov, I.E.; Follath, R.; Gorovikov, S.A.; Püttner, R.; Schmidt, J.-S.; Molodtsov, S.L.; Adamchuk, V.K.; Gudat, W.; et al. Commissioning results and performance of the high-resolution Russian–German beamline at BESSY II. *Nucl. Instrum. Methods Phys. Res. Sect. A Accel. Spectrometers Detect. Assoc. Equip.* **2003**, *505*, 718–728. [[CrossRef](#)]
33. Kummer, K.; Sivkov, V.N.; Vyalikh, D.V.; Maslyuk, V.V.; Blüher, A.; Nekipelov, S.V.; Bredow, T.; Mertig, I.; Mertig, M.; Molodtsov, S.L. Oscillator strength of the peptide bond  $\pi^*$  resonances at all relevant X-ray absorption edges. *Phys. Rev. B* **2009**, *80*, 155433. [[CrossRef](#)]
34. Kroto, H.W.; Allaf, A.W.; Balm, S.P.  $C_{60}$ : Buckminsterfullerene. *Chem. Rev.* **1991**, *91*, 1213–1235. [[CrossRef](#)]
35. Werner, H.; Schedel-Niedrig, T.; Wohlers, M.; Herein, D.; Herzog, B.; Schlögl, R.; Keil, M.; Bradshaw, A.M.; Kirschner, J. Reaction of molecular oxygen with  $C_{60}$ : Spectroscopic studies. *J. Chem. Soc. Faraday Trans.* **1994**, *90*, 403–409. [[CrossRef](#)]
36. Hou, J.G.; Zhao, A.D.; Huang, T.; Lu, S.  $C_{60}$ -based materials. In *Encyclopedia of Nanoscience and Nanotechnology*; Nalwa, H.S., Ed.; American Scientific Publishers: Stevenson Ranch, CA, USA, 2004; Volume 1, pp. 409–474.
37. Rao, A.M.; Zhou, P.; Wang, K.-A.; Hager, G.T.; Holden, J.M.; Wang, Y.; Lee, W.-T.; Bi, X.-X.; Eklund, P.C.; Cornett, D.S.; et al. Photoinduced polymerization of solid  $C_{60}$  films. *Science* **1993**, *259*, 955–957. [[CrossRef](#)]
38. Sundqvist, B. Mapping intermolecular bonding in  $C_{60}$ . *Sci. Rep.* **2015**, *4*, 6171. [[CrossRef](#)] [[PubMed](#)]
39. Leiro, J.A.; Heinonen, M.H.; Laiho, T.; Batirev, I.G. Core-level XPS spectra of fullerene, highly oriented pyrolytic graphite, and glassy carbon. *J. Electron Spectrosc. Relat. Phenom.* **2003**, *128*, 205–213. [[CrossRef](#)]
40. Weaver, J.H.; Martins, J.L.; Komeda, T.; Chen, Y.; Ohno, T.R.; Kroll, G.H.; Troullier, N.; Haufler, R.E.; Smalley, R.E. Electronic structure of solid  $C_{60}$ : Experiment and theory. *Phys. Rev. Lett.* **1991**, *66*, 1741–1744. [[CrossRef](#)]
41. Weaver, J.H. Electronic structures of  $C_{60}$ ,  $C_{70}$  and the fullerenes: Photoemission and inverse photoemission studies. *J. Phys. Chem. Solids* **1992**, *53*, 1433–1447. [[CrossRef](#)]
42. Maxwell, A.J.; Brühwiler, P.A.; Arvanitis, D.; Hasselström, J.; Mårtensson, N. C 1s ionisation potential and energy referencing for solid  $C_{60}$  films on metal surfaces. *Chem. Phys. Lett.* **1996**, *260*, 71–77. [[CrossRef](#)]
43. Jeong, H.-K.; Noh, H.-J.; Kim, J.-Y.; Jin, M.H.; Park, C.Y.; Lee, Y.H. X-ray absorption spectroscopy of graphite oxide. *Europhys. Lett.* **2008**, *82*, 67004. [[CrossRef](#)]
44. Batson, P.E. Carbon 1s near-edge-absorption fine structure in graphite. *Phys. Rev. B* **1993**, *48*, 2608–2610. [[CrossRef](#)] [[PubMed](#)]
45. Rosenberg, R.A.; Love, P.J.; Rehn, V. Polarization-dependent C(K) near-edge X-ray-absorption fine structure of graphite. *Phys. Rev. B* **1986**, *33*, 4034–4037. [[CrossRef](#)] [[PubMed](#)]
46. Skytt, P.; Glans, P.; Mancini, D.C.; Guo, J.-H.; Wassdahl, N.; Nordgren, J.; Ma, Y. Angle-resolved soft-X-ray fluorescence and absorption study of graphite. *Phys. Rev. B* **1994**, *50*, 10457–10461. [[CrossRef](#)]
47. Brühwiler, P.A.; Maxwell, A.J.; Puglia, C.; Nilsson, A.; Andersson, S.; Mårtensson, N.  $\pi^*$  and  $\sigma^*$  excitons in C 1s absorption of graphite. *Phys. Rev. Lett.* **1995**, *74*, 614–617. [[CrossRef](#)] [[PubMed](#)]
48. Mane, J.M.; Le Normand, F.; Medjo, R.E.; Cojocar, C.S.; Ersen, O.; Senger, A.; Laffon, C.; Sendja, B.T.; Biouele, C.M.; Ben-Bolie, G.H.; et al. Alignment of vertically grown carbon nanostructures studied by X-ray absorption spectroscopy. *Mater. Sci. Appl.* **2014**, *5*, 966–983. [[CrossRef](#)]
49. Nyberg, M.; Luo, Y.; Triguero, L.; Pettersson, L.G.M.; Ågren, H. Core-hole effects in X-ray-absorption spectra of fullerenes. *Phys. Rev. B* **1999**, *60*, 7956–7960. [[CrossRef](#)]
50. Wästberg, B.; Lunell, S.; Enkvist, C.; Brühwiler, P.A.; Maxwell, A.J.; Mårtensson, N. 1s X-ray-absorption spectroscopy of  $C_{60}$ : The effects of screening and core-hole relaxation. *Phys. Rev. B* **1994**, *50*, 13031–13034. [[CrossRef](#)] [[PubMed](#)]
51. Krummacher, S.; Biermann, M.; Neeb, M.; Liebsch, A.; Eberhardt, W. Close similarity of the electronic structure and electron correlation in gas-phase and solid  $C_{60}$ . *Phys. Rev. B* **1993**, *48*, 8424–8429. [[CrossRef](#)] [[PubMed](#)]
52. Haddon, R.C. Chemistry of the fullerenes: The manifestation of strain in a class of continuous aromatic molecules. *Science* **1993**, *261*, 1545–1550. [[CrossRef](#)]
53. Haddon, R.C.; Brus, L.E.; Raghavachari, K. Electronic structure and bonding in icosahedral  $C_{60}$ . *Chem. Phys. Lett.* **1986**, *125*, 459–464. [[CrossRef](#)]
54. Fowler, P.W.; Woolrich, J.  $\pi$ -Systems in three dimensions. *Chem. Phys. Lett.* **1986**, *127*, 78–83. [[CrossRef](#)]

55. Saito, S.; Oshiyama, A. Cohesive mechanism and energy bands of solid C<sub>60</sub>. *Phys. Rev. Lett.* **1991**, *66*, 2637–2640. [[CrossRef](#)]
56. Chen, H.S.; Kortan, A.R.; Haddon, R.C.; Fleming, D.A. Thermodynamics of fullerene (C<sub>60</sub>) in pure oxygen, nitrogen and argon. *J. Phys. Chem.* **1992**, *96*, 1016–1018. [[CrossRef](#)]
57. Wohlers, M.; Werner, H.; Belz, T.; Rühle, T.; Schlögl, R. C<sub>60</sub>: A host lattice for the intercalation of oxygen? *Mikrochim. Acta* **1997**, *125*, 401–406. [[CrossRef](#)]
58. Ohno, T.R.; Chen, Y.; Harvey, S.E.; Kroll, G.H.; Weaver, J.H.; Haufler, R.E.; Smalley, R.E. C<sub>60</sub> bonding and energy-level alignment on metal and semiconductor surfaces. *Phys. Rev. B* **1991**, *44*, 13747–13755. [[CrossRef](#)] [[PubMed](#)]
59. Berezkin, V.I.; Viktorovskii, I.V.; Vul', A.Y.; Golubev, L.V.; Petrova, V.N.; Khoroshko, L.O. Fullerene single crystals as adsorbents of organic compounds. *Semiconductors* **2003**, *37*, 775–783. [[CrossRef](#)]
60. Erbahar, D.; Susi, T.; Rocquefelte, X.; Bittencourt, C.; Scardamaglia, M.; Blaha, P.; Guttman, P.; Rotas, G.; Tagmatarchis, N.; Zhu, X.; et al. Spectromicroscopy of C<sub>60</sub> and azafullerene C<sub>59</sub>N: Identifying surface adsorbed water. *Sci. Rep.* **2016**, *6*, 35605. [[CrossRef](#)]
61. Yamamoto, S.; Bluhm, H.; Andersson, K.; Ketteler, G.; Ogasawara, H.; Salmeron, M.; Nilsson, A. In Situ X-ray photoelectron spectroscopy studies of water on metals and oxides at ambient conditions. *J. Phys. Condens. Matter* **2008**, *20*, 184025. [[CrossRef](#)]
62. Henderson, M. The interaction of water with solid surfaces: Fundamental aspects revisited. *Surf. Sci. Rep.* **2002**, *46*, 1–308. [[CrossRef](#)]
63. Hodgson, A.; Haq, S. Water adsorption and the wetting of metal surfaces. *Surf. Sci. Rep.* **2009**, *64*, 381–451. [[CrossRef](#)]
64. Schiros, T.; Andersson, K.J.; Pettersson, L.G.M.; Nilsson, A.; Ogasawara, H. Chemical bonding of water to metal surfaces studied with core-level spectroscopies. *J. Electron Spectrosc. Relat. Phenom.* **2010**, *177*, 85–98. [[CrossRef](#)]
65. Weissenrieder, J.; Mikkelsen, A.; Andersen, J.N.; Feibelman, P.J.; Held, G. Experimental evidence for a partially dissociated water bilayer on Ru{0001}. *Phys. Rev. Lett.* **2004**, *93*, 196102. [[CrossRef](#)] [[PubMed](#)]
66. Carrasco, J.; Hodgson, A.; Michaelides, A. A molecular perspective of water at metal interfaces. *Nat. Mater.* **2012**, *11*, 667–674. [[CrossRef](#)]
67. Kimmel, G.A.; Matthiesen, J.; Baer, M.; Mundy, C.J.; Petrik, N.G.; Smith, R.S.; Dohnálek, Z.; Kay, B.D. No confinement needed: Observation of a metastable hydrophobic wetting two-layer ice on graphene. *J. Am. Chem. Soc.* **2009**, *131*, 12838–12844. [[CrossRef](#)]
68. Sundar, C.S.; Bharathi, A.; Hariharan, Y.; Janaki, J.; Sankara Sastry, V.; Radhakrishnan, T.S. Thermal decomposition of C<sub>60</sub>. *Solid State Commun.* **1992**, *84*, 823–826. [[CrossRef](#)]
69. Warren, B.E. X-ray diffraction in random layer lattices. *Phys. Rev.* **1941**, *59*, 693–698. [[CrossRef](#)]
70. Franklin, R.E. The interpretation of diffuse X-ray diagrams of carbon. *Acta Crystallogr.* **1950**, *3*, 107–121. [[CrossRef](#)]
71. Franklin, R.E. Crystallite growth in graphitizing and non-graphitizing carbons. *Proc. R. Soc. Lond. A* **1951**, *209*, 196–218. [[CrossRef](#)]
72. Davydov, V.A.; Rakhmanina, A.V.; Agafonov, V.; Narymbetov, B.; Boudou, J.-P.; Szwarc, H. Conversion of polycyclic aromatic hydrocarbons to graphite and diamond at high pressures. *Carbon* **2004**, *42*, 261–269. [[CrossRef](#)]
73. Petrenko, I.; Summers, A.P.; Simon, P.; Żółtowska-Aksamitowska, S.; Motylenko, M.; Schimpf, C.; Rafaja, D.; Roth, F.; Kummer, K.; Brendler, E.; et al. Extreme biomimetics: Preservation of molecular detail in centimeter-scale samples of biological meshes laid down by sponges. *Sci. Adv.* **2019**, *5*, eaax2805. [[CrossRef](#)]
74. Kinoshita, K. *Carbon: Electrochemical and Physicochemical Properties*; Wiley: New York, NY, USA, 1988; ISBN 978-0-471-84802-8.
75. Porezag, D.; Pederson, M.R.; Frauenheim, T.; Köhler, T. Structure, stability, and vibrational properties of polymerized C<sub>60</sub>. *Phys. Rev. B* **1995**, *52*, 14963–14970. [[CrossRef](#)] [[PubMed](#)]
76. Moret, R.; Launois, P.; Wågberg, T.; Sundqvist, B.; Agafonov, V.; Davydov, V.A.; Rakhmanina, A.V. Single-crystal structural study of the pressure-temperature-induced dimerization of C<sub>60</sub>. *Eur. Phys. J. B Condens. Matter Complex Syst.* **2003**, *37*, 25–37. [[CrossRef](#)]
77. Moret, R.; Launois, P.; Wågberg, T.; Sundqvist, B. High-pressure synthesis, structural and raman studies of a two-dimensional polymer crystal of. *Eur. Phys. J. B Condens. Matter Complex Syst.* **2000**, *15*, 253–263. [[CrossRef](#)]
78. Davydov, V.A.; Kashevarova, L.S.; Rakhmanina, A.V.; Senyavin, V.M.; Céolin, R.; Szwarc, H.; Allouchi, H.; Agafonov, V. Spectroscopic study of pressure-polymerized phases of C<sub>60</sub>. *Phys. Rev. B* **2000**, *61*, 11936–11945. [[CrossRef](#)]
79. Ferrari, A.C. Raman spectroscopy of graphene and graphite: Disorder, electron–phonon coupling, doping and nonadiabatic effects. *Solid State Commun.* **2007**, *143*, 47–57. [[CrossRef](#)]
80. Sundqvist, B.; Edlund, U.; Jacobsson, P.; Johnels, D.; Jun, J.; Launois, P.; Moret, R.; Persson, P.-A.; Soldatov, A.; Wågberg, T. Structural and physical properties of pressure polymerized C<sub>60</sub>. *Carbon* **1998**, *36*, 657–660. [[CrossRef](#)]
81. Han, S.; Yoon, M.; Berber, S.; Park, N.; Osawa, E.; Ihm, J.; Tománek, D. Microscopic mechanism of fullerene fusion. *Phys. Rev. B* **2004**, *70*, 113402. [[CrossRef](#)]
82. Bagramov, R.; Serebryanaya, N.; Kulnitskiy, B.; Blank, V. C<sub>60</sub> and C<sub>70</sub> pressure-and-temperature transformations into fullerene-related forms. *Fuller. Nanotub. Carbon Nanostruct.* **2016**, *24*, 20–24. [[CrossRef](#)]
83. Sing, M.; Soldatov, A.; Pichler, T.; Sundqvist, B.; Knupfer, M.; Golden, M.S.; Fink, J. Electronic structure studies of pressure-polymerized C<sub>60</sub>. *Synth. Met.* **1999**, *103*, 2454–2455. [[CrossRef](#)]